Monthly Notices
of the
ROYAL ASTRONOMICAL SOCIETY

MNRAS **466,** 1140–1148 (2017)
Advance Access publication 2016 December 7

doi:10.1093/mnras/stw3159

Constraining the PopIII IMF with high-z GRBs

Q. Ma,[1,2,3⋆] U. Maio,[4] B. Ciardi[1] and R. Salvaterra[5]

[1]*Max-Planck-Institut für Astrophysik, Karl-Schwarzschild-Straße 1, D-85748 Garching bei München, Germany*
[2]*Purple Mountain Observatory, Chinese Academy of Sciences, Nanjing 210008, China*
[3]*University of Chinese Academy of Sciences, Beijing 100049, China*
[4]*Leibniz-Institut für Astrophysik, An der Sternwarte 16, D-14482 Potsdam, Germany*
[5]*INAF, IASF Milano, via E. Bassini 15, I-20133 Milano, Italy*

Accepted 2016 December 2. Received 2016 December 1; in original form 2016 June 12

ABSTRACT

We study the signatures of enrichment from PopIII stars in observations of PopII GRBs (GRBIIs) at high redshift by using numerical N-body/hydrodynamical simulations including atomic and molecular cooling, star formation and metal spreading from stellar populations with different initial mass functions (IMFs), yields and lifetimes. PopIII and PopII star formation regimes are followed simultaneously and both a top-heavy and a Salpeter-like IMF for pristine PopIII star formation are adopted. We find that the fraction of GRBIIs hosted in a medium previously enriched by PopIII stars (PopIII-dominated) is model-independent. Typical abundance ratios, such as [Si/O] versus[C/O] and [Fe/C] versus[Si/C], can help to disentangle enrichment from massive and intermediate PopIII stars, while low-mass first stars are degenerate with regular PopII generations. The properties of galaxies hosting PopIII-dominated GRBIIs are not very sensitive to the particular assumption on the mass of the first stars.

Key words: gamma-ray burst: general – stars: Population III – cosmology: theory – dark ages, reionization, first stars – early Universe.

1 INTRODUCTION

Long gamma-ray bursts (GRBs) are believed to arise from the accretion of material on to black holes (BHs) formed after the death of massive stars. Some of them are so bright that they have been observed up to extremely high redshift (Salvaterra et al. 2009; Tanvir et al. 2009; Cucchiara et al. 2011). In fact, different models (Bromm & Loeb 2002; Salvaterra & Chincarini 2007; de Souza, Yoshida & Ioka 2011; Salvaterra et al. 2012; Elliott et al. 2015; Ghirlanda et al. 2015) consistently predict that ∼3 per cent of the GRBs detected by the *Swift* satellite should lie at $z > 6$. Among these, some might also be GRBs from the earliest generation (PopIII) of stars (Suwa & Ioka 2011; Toma, Sakamoto & Mészáros 2011; Maio & Barkov 2014). Therefore, high-z GRBs are thought to be a viable probe of the early Universe besides quasars and galaxies (see Salvaterra 2015, for a recent review). Indeed, they can pin-point the primordial galaxies (Koopmans et al. 2015) responsible for the reionization of the intergalactic medium (Salvaterra et al. 2013), providing unique information about their gas metallicity and dust content (Campisi et al. 2011), neutral hydrogen fraction (Nagamine, Zhang & Hernquist 2008), local intergalactic radiation field (Inoue et al. 2010) and stellar populations (Ma et al. 2015). Moreover, they could add constraints to early cosmic magnetic fields (Takahashi et al. 2011), dark matter nature (de Souza et al. 2013b; Maio & Viel 2015) and primordial non-Gaussianities (Maio 2011; Maio et al. 2012). The detection of a PopIII GRB (hereafter GRBIII) will represent a breakthrough for our knowledge of the early phases of star formation in the Universe. Previous theoretical estimates (Maio & Barkov 2014) have shown that powerful GRBs originated by very massive first stars contribute about 1 percent of the total GRB rate at $z \simeq 6$ and less than 0.1 percent at low redshift, representing only 1/10th of the entire pristine GRBIII population (Campisi et al. 2011). Therefore, GRB samples with at least hundreds of events at $z \gtrsim 6$ and thousands events at later epochs will be strongly required in future observational campaigns to detect such extreme objects.

However, with the exception of the highest redshifts, the GRBIII rate is expected to be much lower than the rate of PopII GRBs (hereafter GRBIIs), because of the minor PopIII contribution to the cosmic star formation rate (SFR) density (Salvaterra et al. 2013). For this reason, it will be more likely to detect signatures of first stars with GRBIIs rather than directly with GRBIIIs.[1] Indeed, the afterglow of GRBs, expected to be visible up to very high redshift (e.g. Ciardi & Loeb 2000), carries information about the

⋆ E-mail: maqb@mpa-garching.mpg.de.

[1] None the less, in selected cases, i.e. very massive PopIII stars, the GRBIII rate may be comparable to that of GRBII that form in a medium enriched by PopIII stars (Ma et al. 2015).

surrounding interstellar medium (ISM) through measurements of the metal abundance ratios. For example, GRB 130606A at $z = 5.91$ has been observed in the full optical and near-IR wavelength region at intermediate spectral resolution with VLT/X-shooter (Hartoog et al. 2015). The spectrum has very high S/N ratio with many metal absorption lines detected. Indirect signatures of the first stars can be identified by exploring the gas enrichment patterns around GRBIIs (Salvaterra et al. 2013; Ma et al. 2015). GRBIIs formed in an environment pre-enriched by massive PopIII stars (referred to as GRBII→III in Ma et al. 2015) are expected to be preferentially hosted in galaxies with SFR $\sim 10^{-3}$–$10^{-1}\,M_\odot\,yr^{-1}$ and metallicity $Z \sim 10^{-4}$–$10^{-2}\,Z_\odot$, lower than those of normal high-z galaxies (de Souza et al. 2013a; Salvaterra et al. 2013).

Compared to other indirect detection techniques of first stars, e.g. very metal-poor (VMP) and extremely metal-poor (EMP) stars, and also damped Lyman-α absorbers (DLA; see review e.g. Nomoto, Kobayashi & Tominaga 2013), observations of GRBs can extend to very high redshift, where the contribution of first stars is more significant (Ma et al. 2015). Indeed, GRBs have been observed at $z > 9$ (Cucchiara et al. 2011). Instead, because of their faint luminosity, VMP and EMP stars are only observed in our Milky Way and nearby dwarf galaxies. Even so, their metal abundances could be representative of a single (or a few) supernovae (SNe) episode from first star, at least for the few cases in which the total metallicity is below the critical value, e.g. the Caffau et al. (2011) star. In principle, measurements of the abundance ratios in EMP stars could provide a hint about the initial mass function (IMF) of PopIII stars. Also DLAs are observed at high redshift, up to $z \sim 7$ (Becker et al. 2012; Simcoe et al. 2012), but their number depends on the density of background quasars, which are very rare at $z > 10$.

However, the metal yields from PopIII SN explosions depend strongly on the properties of their progenitor star (Heger & Woosley 2002, 2010), and are thus highly uncertain, because of our persistent ignorance of the typical mass of PopIII stars, which in the current literature is predicted to be both large (e.g. Heger & Woosley 2002; Schneider et al. 2002; Suda & Fujimoto 2010) and small (e.g. Clark et al. 2011; Stacy & Bromm 2014). To improve our knowledge in this respect, here we run numerical hydrodynamical chemistry simulations with different PopIII IMFs and study how gas pollution of GRBII hosts is affected by these changes. The brightness of GRBs that can be observed by *Swift*/Burst Alert Telescope (BAT) and also the predicted observable GRB rate relating to first stars have been studied in Campisi et al. (2011) and Ma et al. (2015), e.g. $\sim 0.06\,yr^{-1}\,sr^{-1}$ of PopIII star enriched GRBIIs should be bright enough to trigger *Swift*/BAT. In this paper, we focus on the effect of different first star IMFs on the fraction of GRBIIs triggered in a medium enriched by PopIII stars, and on the properties of GRBII host galaxies. We will also show how metal abundance ratios detectable in the GRB afterglow spectra of current or future spectroscopic observations can help in discriminating among different PopIII IMFs.

Throughout this work, a standard ΛCDM cosmological model is adopted with the following parameters: cosmological constant density parameter $\Omega_{0,\Lambda} = 0.7$, total matter density parameter $\Omega_{0,M} = 0.3$, baryon matter density $\Omega_b = 0.04$, primordial spectral index $n = 1$, cosmic variance within a sphere of 8 $kpc\,h^{-1}$ radius $\sigma_8 = 0.9$ and expansion parameter $h = 0.7$ in units of $100\,km\,s^{-1}\,Mpc^{-1}$. This paper is organized as follows: the simulations we used are described in Section 2, as well as the classification for gas particles; we present our results in Section 3; we critically discuss the caveats of our approach and give our conclusions in Section 4.

Table 1. From left to right the columns refer to: model name, stellar mass range for the PopIII IMF, stellar mass range for SN explosions and stellar mass range for the PopII IMF.

Model	PopIII range ($M_\odot$)	SN range ($M_\odot$)	PopII range ($M_\odot$)
VMSN	100–500	140–260	0.1–100
MSN	0.1–100	10–100	0.1–100
RSN	0.1–100	10–40	0.1–100

2 SIMULATIONS

The code used here is a modified version of GADGET2 code (Springel 2005) based on our previous works (see e.g. Maio et al. 2007, 2010; Tornatore et al. 2007b; Maio, Ciardi & Müller 2013a, for further details) and, besides gravity and hydro, it follows atomic and molecular cooling based on H, He, H_2, HD, stellar evolution and metal pollution for various heavy elements (C, N, O, Ne, Mg, Si, S, Ca, Fe, etc.). To describe physical processes in the ISM that are not directly resolved in the simulation, e.g. star formation in gas particles and feedback from stars, a subgrid model has been adopted. At the end of their lifetimes, which depend on the stellar mass, the stars explode and spread metals and energy into gas neighbours according to the SPH kernel (Tornatore et al. 2007b).

We run three simulations with different PopIII IMFs, which are referred to as Very Massive SN (VMSN), Massive SN (MSN) and Regular SN (RSN), as listed in Table 1. The box side length is $10\,Mpc\,h^{-1}$ with particles number 2×320^3, yielding a gas and dark matter particle mass of $3.39 \times 10^5\,M_\odot\,h^{-1}$ and $2.20 \times 10^6\,M_\odot\,h^{-1}$, respectively. All models adopt IMFs with Salpeter slope, but they differ in the lower/upper mass limits and the range of masses contributing to metal pollution. In the VMSN model, the first stars are assumed to be very massive, in the range [100, 500] $M_\odot$, while the stars contributing to metal spreading are the progenitors of Pair-Instability Supernovae (PISN) in the mass range [140, 260] $M_\odot$ (Heger & Woosley 2002). Both MSN and RSN models have a PopIII IMF covering masses over [0.1, 100] $M_\odot$. In the RSN case, PopIII stars with mass [40, 100] $M_\odot$ are assumed to collapse directly into BHs, so that the only contribution to metal enrichment comes from the mass range [10, 40] $M_\odot$ (Woosley & Weaver 1995; Heger & Woosley 2002). In the MSN scenario, instead, stars with masses in the range [40, 100] $M_\odot$ also contribute to metal pollution by exploding as core-collapse SNe (Heger & Woosley 2010). For PopII stars, we adopt a Salpeter IMF in the mass range [0.1, 100] $M_\odot$ in all the simulations.

The various metal yields are tracked during the simulations and summed up to give the total metallicity Z of each star or gas particle. The transition from a PopIII to a PopII/I star formation regime is dictated by the local gas metallicity. More specifically, PopIII (PopII/I) stars are formed at metallicities below (above) $10^{-4}\,Z_\odot$ (Schneider et al. 2002, 2003). For PopII stars, we include metal yields from AGBs (van den Hoek & Groenewegen 1997), Type Ia SNe (SNIa; Thielemann et al. 2003) and Type II SNe (SNII; Woosley & Weaver 1995).

Metal pollution by PopIII stars is followed separately from that by PopII/I stars. More specifically, for each gas particle in the simulated boxes, the fraction of metals produced by PopIII stars is defined as

$$f_{\rm III} = \frac{\sum_j m_{Z_j,{\rm III}}}{\sum_j m_{Z_j}}, \quad (1)$$

where m_{Z_j} is the mass of metal element Z_j in the gas particle, while $m_{Z_j,{\rm III}}$ is the mass coming from PopIII stars. Here, Z_j indicates all heavy elements except from hydrogen and helium. According to the

value of $f_{\rm III}$, we assign each gas particle with non-zero Z to one of the following three classes:

(i) PopII-dominated, if $f_{\rm III} < 20$ per cent;
(ii) intermediate, if 20 per cent $< f_{\rm III} < 60$ per cent;
(iii) PopIII-dominated, if $f_{\rm III} > 60$ per cent.

We have verified that the exact boundaries chosen for the class definition (e.g. ± 10 per cent) do not have a relevant impact on the results presented in the paper.

3 RESULTS

In the following, we analyse the simulations and show results of the GRB rate evolution, the probability distribution of different class of GRBIIs given one or two metal abundance ratios, and also the properties of GRB host galaxies in the three models.[2] For the metal abundance, we only consider selected elements, such as carbon (C), oxygen (O), silicon (Si) and iron (Fe), since these are the most abundant in the Universe and easier to detect in the spectra of high-z GRB afterglows (Kawai et al. 2006; Castro-Tirado et al. 2013). Sulphur (S) always follows Si and shows a similar behaviour.

Quantitatively, metal abundance ratios with respect to the solar values are defined as

$$[{\rm A/B}] = \log_{10}(N_{\rm A}/N_{\rm B}) - \log_{10}(N_{\rm A}/N_{\rm B})_{\odot}, \quad (2)$$

where A and B are two arbitrary species, $N_{\rm A(B)}$ is the number density of element A(B), and the subscript $\odot$ denotes the solar values from Asplund et al. (2009).

3.1 GRB rate evolution

At any given redshift, the comoving GRBII rate density in class i subsample (i.e. PopII-dominated, intermediate or PopIII-dominated) is calculated as in Campisi et al. (2011) and Ma et al. (2015; hereafter referred to as Ma2015):

$$\rho_{{\rm GRBII},i}(z) = f_{\rm GRBII}\ \zeta_{\rm BHII}\ \rho_{\star,i}(z), \quad (3)$$

where $f_{\rm GRBII}$ is the fraction of BHs that ignites a GRBII, $\zeta_{\rm BHII}$ is the fraction of BHs formed per unit of PopII/I stellar mass, and $\rho_{\star,i}$ is the comoving SFR density of class i subsample at redshift z. We adopt $f_{\rm GRBII} = 0.028$ and $\zeta_{\rm BHII} = 0.002$ following Campisi et al. (2011) and Ma2015. It should be noted that, since GRBs are related to the death of massive stars, in our calculations we include only gas particles with non-zero SFR.

In Fig. 1, we show the redshift evolution of the fraction r_i of GRBII rate that is class i:

$$r_i(z) = \frac{\rho_{{\rm GRBII},i}(z)}{\rho_{\rm GRBII,tot}(z)}, \quad (4)$$

where $\rho_{\rm GRBII,\,tot}(z)$ is the total comoving GRBII rate density at redshift z. In the figure, solid, dashed and dotted lines refer to VMSN, MSN and RSN, respectively. The three models show a similar evolution, with the contribution of the PopIII-dominated class decreasing dramatically with redshift, with a fraction of about 1 at $z \gtrsim 17$, but only $\sim 10^{-2}$ at $z = 6$. This is a consequence of the efficient metal enrichment in the early episodes of structure formation. Indeed, after a first short period in which PopIII events in pristine molecular-driven star-forming regions dominate, they rapidly leave room to following generations formed in the recently polluted material. Interestingly, although the PopIII SFR is somewhat affected by the PopIII stellar properties (Maio et al. 2010, 2016), the resulting trends are not very sensitive to the scenarios adopted for the first stars IMF. The three cases evolve quite closely, with only a minor delay in the RSN scenario, due to the longer stellar lifetimes and later spreading events (consistently with SN ranges in Table 1). The small differences between the trends for VMSN and MSN are due to the different SN explosion energies (lifetimes are comparable), which imply slightly more local enrichment (hence lower PopIII contribution) in the MSN case. For VMSN, metals are spread further away from star-forming sites and more diluted within the hosting halo.

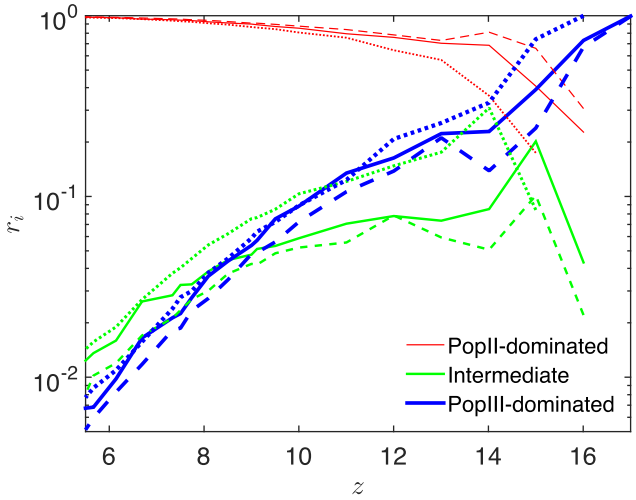

Figure 1. Fraction of GRBII rate that comes from PopII-dominated (thin red lines), intermediate (green) and PopIII-dominated (thick blue) gas as a function of redshift z. Solid, dashed and dotted lines denote VMSN, MSN and RSN.

The contribution of the intermediate class is always between a few per cents and ~20 per cent, with a sharp peak at $z \sim 13$–15 and a subsequent mild drop. This shape is led by the quick, although transitory, phase of early PopIII enrichment ($f_{\rm III} > 60$ per cent) at $z \gtrsim 15$. The first explosions from short-lived stars rapidly enrich the local medium, and the ongoing spreading events from the newly born PopII stars push $f_{\rm III}$ below the 60 per cent threshold (equation 1), causing the steep increase in the figure (green lines). Due to the increasingly larger amount of metals being expelled from PopII/I stars with decreasing redshift, the values of $f_{\rm III}$ for many star-forming gas particles drop below 20 per cent. Thus, the contribution associated with the intermediate class (20 per cent $< f_{\rm III} < 60$ per cent) start to smoothly decrease at $z < 15$.

The trend of the PopII-dominated class is complementary to that of the intermediate and PopIII-dominated ones, and gradually kicks in as an increasingly larger fraction of the gas has PopII progenitors due to metal spreading and stellar evolution, i.e. $r_{\rm PopII-dominated}$ increases quickly with decreasing redshift, and it approaches unity for $z \lesssim 6$.

We note that current data at $z \sim 6$ do not show clear signatures of PopIII-dominated GRBIIs (Ma2015) and this is in agreement with the results of Fig. 1 for $r_{\rm PopIII-dominated}$.

With the integration of $\rho_{\rm GRBII,\,i}(z)$ along the line of sight, we get the total GRBII number of each class at $z > 5.5$, which is listed in Table 2. The three simulations show very similar results, i.e.

[2] While in principle metal absorption observed in the afterglow of GRBs may be due to either the IGM or the ISM, here we assume that it is representative of the host physical properties.

Table 2. Number of class i GRBIIs at $z > 5.5$ predicted in model VMSN, MSN and RSN.

	VMSN	MSN	RSN
PopIII-dominated ($yr^{-1}sr^{-1}$)	6.8×10^3	5.5×10^3	7.0×10^3
Intermediate ($yr^{-1}sr^{-1}$)	7.7×10^3	6.0×10^3	9.9×10^3
PopII-dominated ($yr^{-1}sr^{-1}$)	2.8×10^5	2.8×10^5	2.7×10^5

$\sim 2.8 \times 10^5$ yr^{-1} sr^{-1} PopII-dominated GRBIIs, $\sim 8 \times 10^3$ yr^{-1} sr^{-1} intermediate GRBIIs and $\sim 6 \times 10^3$ yr^{-1} sr^{-1} PopIII-dominated GRBIIs at $z > 5.5$. Because of the limited jet angle of GRBs and also the sensitivity threshold of telescopes, only a small fraction of bright GRBs is observable at high redshift (see further discussion in Campisi et al. 2011), but even if only 0.1 per cent or less of such GRBs were detected, they would open an important observational window on the first stars.

3.2 Disentangling first stars models

We discuss here how we can identify PopIII star signals on the basis of the metal abundance ratios measured in the spectra of high-z GRB optical/NIR afterglows. We also discuss which are the most suitable ratios to look at for constraining the PopIII IMF.

3.2.1 Single metal abundance ratio

We start considering the possibility to identify a PopIII-dominated GRBII from a single metal abundance ratio. Indeed, the measure of two or more ratios may be challenging for very high-z objects, requiring deep NIR spectroscopy early after the GRB event.

The probability distribution of PopIII-dominated GRBIIs at $z \gtrsim 5.5$ as a function of one given abundance ratio, i.e. the Probability Density Function (PDF), is given by

$$P_i(x) = \frac{1}{\int_x \delta\rho_{\mathrm{GRBII},i}(x)} \frac{\delta\rho_{\mathrm{GRBII},i}(x)}{\delta x}, \quad (5)$$

where x denotes one abundance ratio and $\delta\rho_{\mathrm{GRBII},i}(x)$ is the class i GRBII rate density in the interval $[x, x + \delta x]$.

In Fig. 2, we show the probability distributions of [Fe/O], [Si/O], [C/O], [Si/Fe], [Fe/C] and [Si/C] for PopIII-dominated GRBIIs in the VMSN, MSN and RSN case. As a reference, we also plot the distribution for PopII-dominated GRBIIs in each panel (the PopII-dominated PDF coincides in the three cases). We note here that, since the PDFs are normalized to their total rate (see equation 5), PopII-dominated GRBIIs always overwhelm in number than the PopIII-dominated ones. Therefore, to safely identify PopIII-dominated GRBIIs we should rely only on metal abundance ratio ranges where PopII-dominated GRBIIs are not present.

Let us analyse Fig. 2 in more detail. We note that PopII-dominated and PopIII-dominated GRBIIs cover the same range in the [C/O] and [Si/Fe] panels. Therefore, these abundance ratios are not suitable to disentangle PopIII-dominated GRBs in any of our models. The VMSN model shows always the smallest dispersion with a sharp peak at [Fe/O] ≈ -0.2, [Si/O] ≈ 0.5 and [C/O] ≈ -0.6. This is consistent with what found by Ma2015 (see their fig. 4). Although the presence of a peak in the probability distribution is a unique feature of the VMSN model, in most cases this cannot be identified because it is swamped by normal PopII-dominated GRBIIs. Therefore, the only unique signature for selecting PopIII-dominated GRBIIs is [Si/C] > 0.7, as this characterizes at least 94 per cent of PopIII-dominated GRBIIs.

The SN explosions of massive PopIII stars ($> 40\,M_\odot$) in the MSN model produce very low iron and silicon yields, but very high carbon and oxygen yields, so that PopIII-dominated GRBIIs in this model peak at very low [Fe/O], [Si/O] and [Fe/C], and can be identified by e.g. [Fe/O] < -1.5, [Si/O] < -1 or [Fe/C] < -0.8. Each of these criteria can discern at least 50–60 per cent of PopIII-dominated GRBIIs. Since the MSN model also includes the contribution from low-mass PopIII stars (with mass $< 40\,M_\odot$), it has the largest dispersion in each panel.

Finally, PopIII-dominated GRBIIs in the RSN model have a metal abundance distribution very similar to that of PopII-dominated GRBIIs. Although their distributions are visibly shifted compared to those of PopII-dominated GRBIIs, e.g. in the panel of [Si/O], [C/O] and [Si/C], it would be very difficult to distinguish them from the dominating PopII enriched GRBs.

3.2.2 Two metal abundance ratios

Although we have shown that a single metal abundance ratio could be enough to distinguish PopIII-dominated GRBIIs, their identification would be much easier and more efficient if two or more abundance ratios can be measured.

Fig. 3 shows the probability density function of hosting a GRBII in environments with given abundance ratios and contribution to metallicity from PopIII stars at redshift $z \gtrsim 5.5$:

$$P_i(x, y) = \frac{1}{\int_x \int_y \delta\rho_{\mathrm{GRBII},i}(x, y)} \frac{\delta\rho_{\mathrm{GRBII},i}(x, y)}{\delta x \delta y}, \quad (6)$$

where (x, y) indicate any couple of abundance ratios, while $\delta\rho_{\mathrm{GRBII},i}(x, y)$ is the class i GRBII rate density in the interval $\delta x \times \delta y$ centred in (x, y). Contour levels for probabilities of 25, 75 and 100 per cent[3] are shown. Left-, central and right-hand columns refer to VMSN, MSN and RSN scenarios. Upper, middle and lower rows refer to the bivariate probability distributions for [Si/O] versus[C/O], [Fe/C] versus [Si/C] and [Si/O] versus [O/H], respectively. We note that, since only two metal elements are necessary to plot [Si/O] versus [O/H], the challenge in producing an observational [Si/O] versus [O/H] plot could be the same as that of one single metal abundance ratio, i.e. [Si/O].

Let us consider how different classes of GRBIIs populate the abundance ratio planes for our three simulation runs. We note that the contours for PopII-dominated GRBIIs look very similar in all models, as their metal signature is only little affected (<20 per cent) by PopIII metal enrichment. In general, the panel [Si/O] versus [C/O] displays [Si/O] values following a roughly linear relation with [C/O], with a peak probability located around [C/O] $= -0.43$ and [Si/O] $= -0.05$. The highest probability in the [Fe/C] versus [Si/C] panels is around solar [Fe/C] and slightly supersolar [Si/C]. The [Si/O] ratios evolve as the local metallicity tracked by [O/H] increases, and they converge to [Si/O] $\simeq -0.05$ for metallicities [O/H] above > -2.

In the VMSN model, PopIII-dominated GRBIIs are located in the upper-left corner of the plane [Si/O] versus [C/O], and can be distinguished from PopII-dominated GRBIIs by selecting those with [Si/O] >0.67 [C/O] $+ 0.57$ (black dashed line in the figure). The highest probability to identify a PopIII-dominated GRBII is found around [C/O] ~ -0.62 and [Si/O] ~ 0.51 (almost 75 per cent), which is consistent with the critical conditions [C/O] < -0.5 and

[3] The actual value of the 100 per cent contours is ~99.8 per cent since in Fig. 3 we removed particles that are very far away from others.

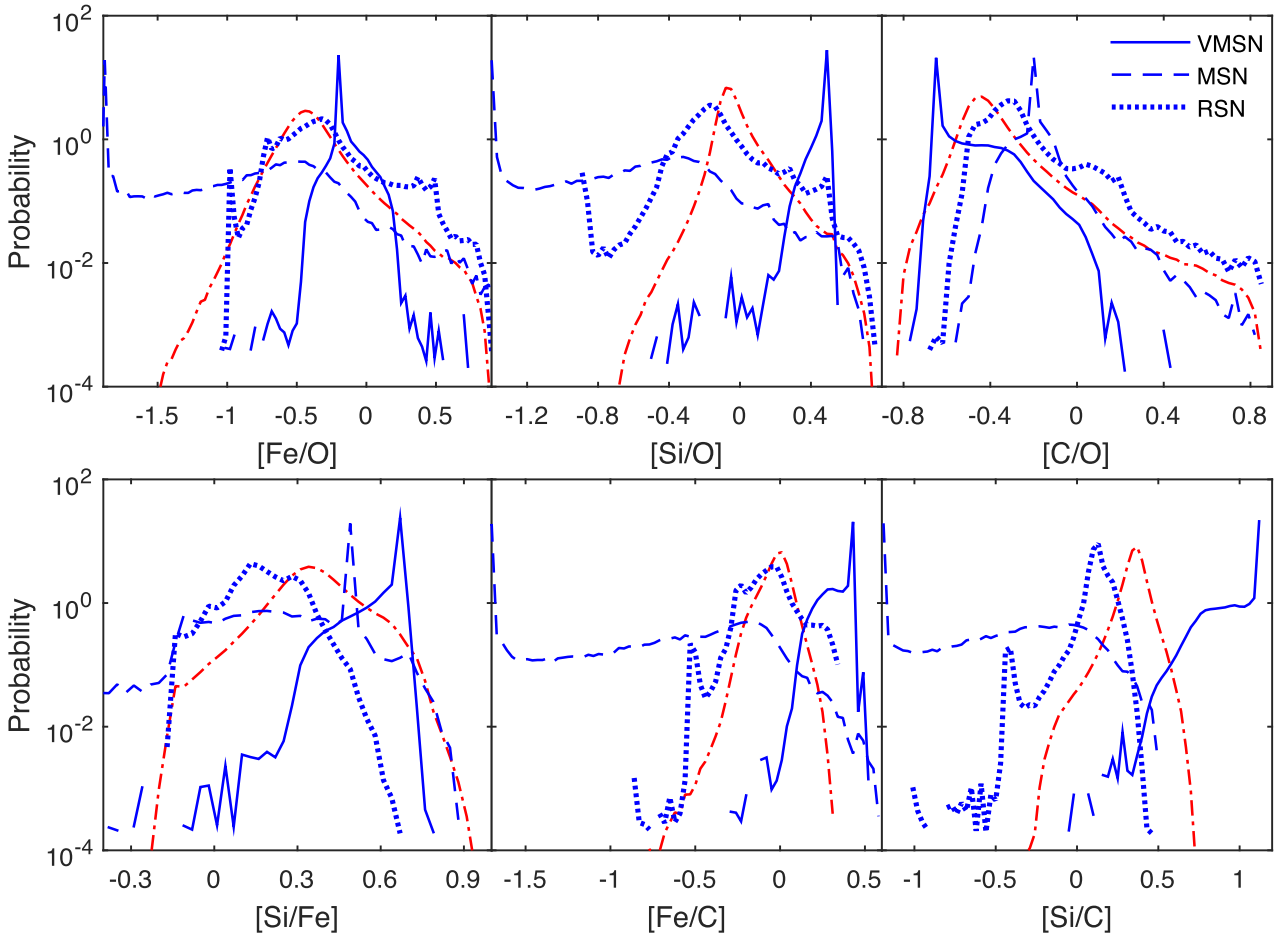

Figure 2. Probability distribution of PopIII-dominated GRBIIs given only one abundance ratio (from left to right and top to bottom, it is [Fe/O], [Si/O], [C/O], [Si/Fe], [Fe/C] and [Si/C]) in model VMSN (solid blue lines), MSN (dashed blue lines) and RSN (dotted blue lines). As a reference, the PDF of PopII-dominated GRBIIs is shown as dash–dotted red line in each panel. Note that the PDFs are normalized by the total rate in each class i and therefore, in number, PopII-dominated GRBIIs overwhelm the distribution of PopIII-dominated ones.

[Si/O] > 0 used in Ma2015 to select GRBIIs enriched by PopIII stars. These can also be identified by selecting [Fe/C] > -1.1 [Si/C] $+ 0.72$ (black dashed line in the figure), where the probability peaks at [Si/C] ~ 1.11 and [Fe/C] ~ 0.43. The panel [Si/O] versus [O/H] is not able to discriminate PopIII-dominated from PopII-dominated GRBIIs, since the distribution of the latter completely encloses the one of the former.

In the MSN model, [Si/O] and [C/O] values of the PopIII-dominated GRBIIs (upper-central panel) have a partial overlap with the PopII-dominated class, although they are also located in different regions. More specifically, at least 70 per cent of them have [Si/O] < 0.83 [C/O] $- 0.38$, since metal yields from PopIII stars with mass [40, 100] $M_\odot$ have high carbon over oxygen yields, but low silicon and iron (Heger & Woosley 2010). The highest probability is around [C/O] $= -0.19$ and [Si/O] $= -1.37$. The tail distribution of low [Si/C] and [Fe/C] can also be distinguished in the panel [Fe/C] versus [Si/C], with [Fe/C] < -1.6 [Si/C] $- 0.54$. The peak values for the PopIII-dominated objects in the [Si/O] versus [O/H] panel have [Si/O] < -1.2, because the [Si/O] ratio of the metal yields from PopIII stars in the MSN model is much lower than that from PopII/I stars (which have [Si/O] $\simeq 0$), thus the two classes are completely decoupled in such regimes.

In the RSN scenario, the metal yields of PopIII stars are very similar to those from PopII/I stars. As a consequence, the contours of PopIII-dominated class overlap with those of other classes, especially the 100 per cent level, while we can still see some visible, albeit modest, shift for the 25 and 75 per cent contour levels in the same direction as in the MSN case.

Finally, GRBIIs of intermediate class are found to lie between those of the PopII- and PopIII-dominated class in each model.

Irrespectively from the adopted IMF, PopIII-dominated GRBIIs are always found in the low-metallicity range, i.e. at [O/H] $\lesssim -2.0$ (at least for 75 per cent contours) since O traces total metallicity (roughly speaking, about 2/3 of heavy elements is in oxygen species). Going to higher [O/H] values, GRBIIs belong to the intermediate- and PopII-dominated class. This evolution from PopIII- to PopII-dominated class in the different scenarios can be read as a consequence of ongoing mechanical and chemical feedback in the Universe (Maio et al. 2011), which increases the local enrichment level according to the corresponding stellar evolution time-scales.

In the panels [Si/O] versus [C/O] and [Fe/C] versus [Si/C], we also show the corresponding IMF-integrated values of the stellar yields from PopIII stars in different models (blue pentagrams) and PopII/I stars (red hexagrams). These values could in principle be used to vaguely identify signatures of PopIII stars, although they rest on limited modelling.

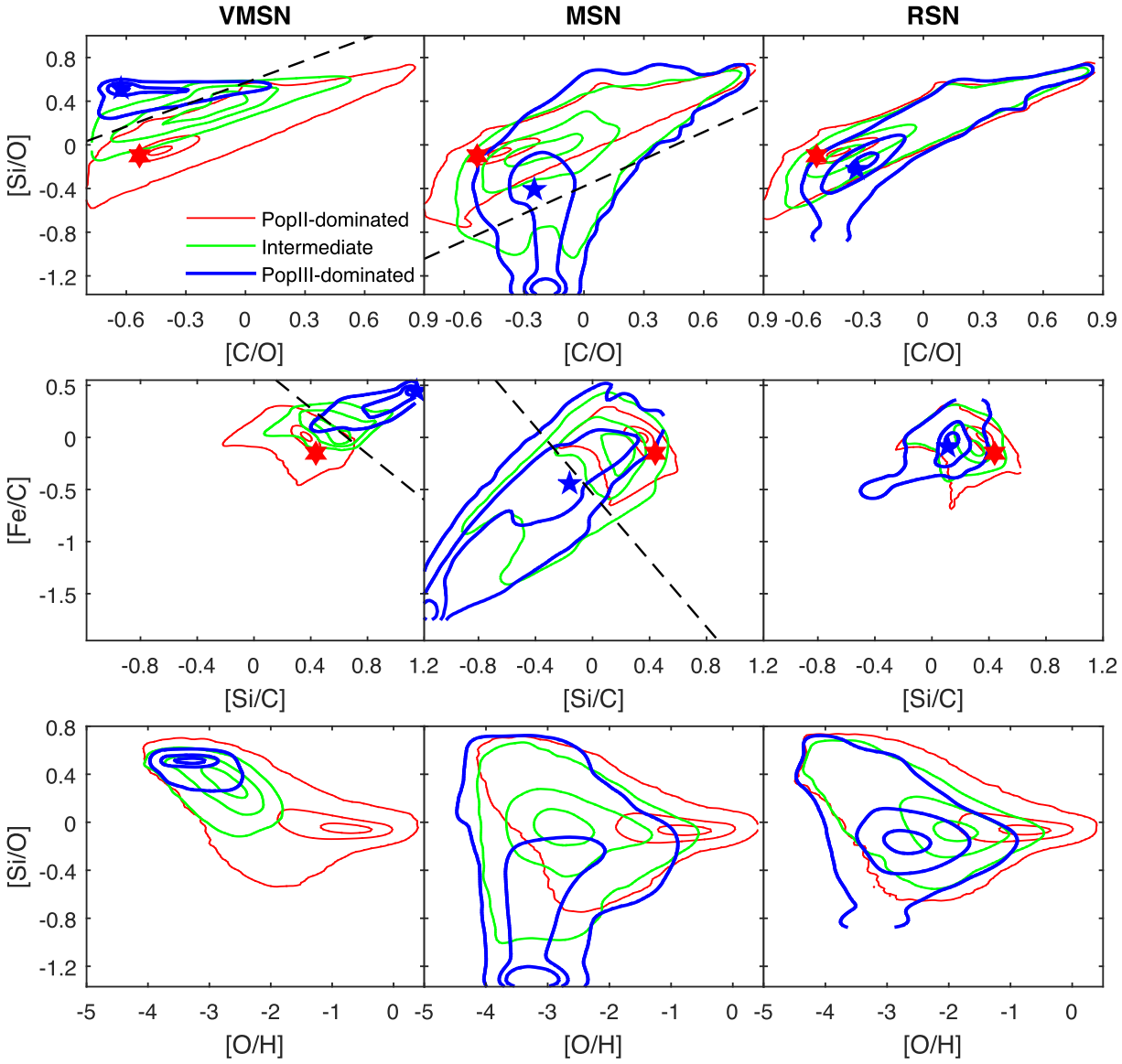

Figure 3. Probability of a class *i* GRBII to have two given abundance ratios in the plane [Si/O] versus [C/O] (top panels), [Fe/C] versus [Si/C] (middle) and [Si/O] versus [O/H] (bottom), for VMSN, MSN and RSN (from left to right) and PopII-dominated (thin red lines), intermediate (green) and PopIII-dominated (thick blue) class. The contours of each colour refer to a probability of 25, 75 and 100 per cent from the innermost to the outermost. The black dashed line in the upper-left panel corresponds to [Si/O] = 0.67 [C/O] + 0.57, the one in the upper-central panel to [Si/O] = 0.83 [C/O] − 0.38, the one in the middle-left panel to [Fe/C] = −1.1 [Si/C] + 0.72, and the one in the middle central panel to [Fe/C] = −1.6 [Si/C] − 0.54. The blue pentagrams and red hexagrams denote the IMF-integrated abundance ratios of the stellar yields from PopIII stars and PopII/I stars, respectively.

The distribution of abundance ratios, as those obtained with our simulations, are much more powerful tools to characterize environments and yields from different stellar populations. In fact, the advantage of our simulations is that they include a series of physical processes (unaccounted for by simple IMF integration) that could affect the distributions of GRBIIs and their abundance ratio patterns, e.g. star formation, feedback effects, transition between PopIII and PopII regime, metallicity-dependent stellar lifetimes, metal spreading and so on. On the contrary, the IMF integration only gives one point for each abundance ratio (as shown in Fig. 3).

3.3 GRB host properties

In Fig. 4, we show the PopIII-dominated and PopII-dominated SFR weighted distributions of the properties of GRBII host galaxies in the three models. We focus on total metallicity Z (top panels), stellar mass $M_\star$ (middle) and SFR (bottom). As in Ma2015, the weights to the corresponding distributions are computed as $\mathrm{SFR}_{i,k}/\mathrm{SFR}_{i,\mathrm{tot}}$, where $\mathrm{SFR}_{i,k}$ is the total class i SFR of galaxies in the kth bin, and $\mathrm{SFR}_{i,\mathrm{tot}}$ is the integral of class i SFR over all galaxies. Here, we include all the host galaxies at redshift $z \gtrsim 5.5$. In each panel of the figure, the blue dashed line shows the probability for a GRBII hosted in a given galaxy to be PopIII-dominated, i.e. $\mathrm{SFR}_{i,\,k}/\mathrm{SFR}_{\mathrm{tot},k}$, where $\mathrm{SFR}_{\mathrm{tot},k}$ is the total SFR of galaxies in the kth bin.

A simple example can better clarify this: let us consider the VMSN model distribution in terms of SFR (bottom-left box). Although the PopIII-dominated GRBII distribution (solid black line) peaks at SFR $\sim 10^{-2}\,\mathrm{M}_\odot\,\mathrm{yr}^{-1}$, the probability to find a PopIII-dominated GRBII in a galaxy (dashed blue) with SFR $\sim 10^{-2}\,\mathrm{M}_\odot\,\mathrm{yr}^{-1}$ is only 20 per cent. On the other hand, while a

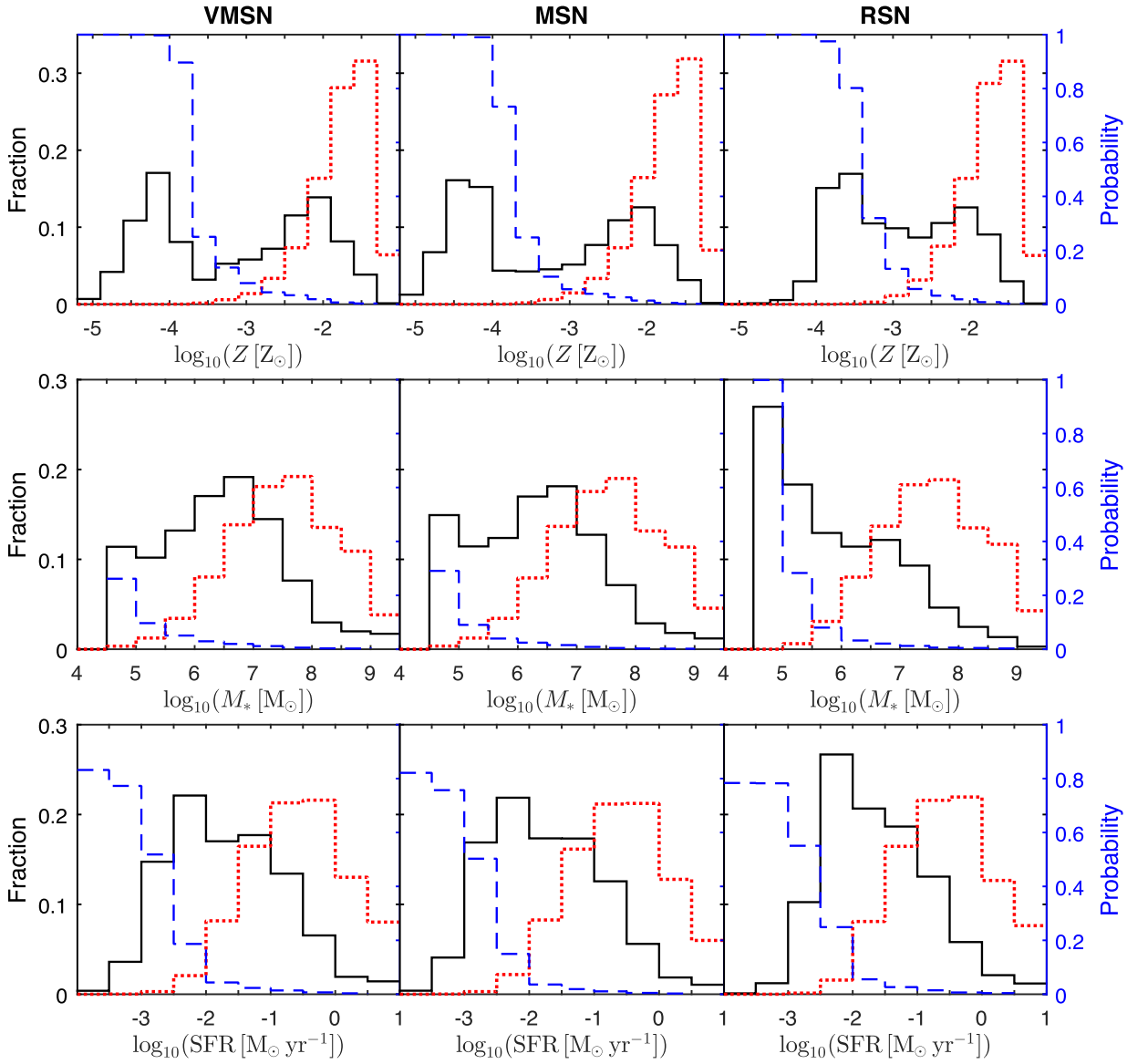

Figure 4. From top to bottom, metallicity, stellar mass and SFR distribution of galaxies hosting GRBIIs. The solid black (dotted red) lines are the distributions of galaxies weighted by the PopIII-dominated (PopII-dominated) PopII SFR; while the dashed blue lines refer to the probability for a GRBII hosted in a given galaxy to be PopIII-dominated. From left to right, the columns refer to model VMSN, MSN and RSN.

rarer event, the identification of a GRBII in a galaxy with SFR $\leq 10^{-3}\,\mathrm{M}_\odot\,\mathrm{yr}^{-1}$ would clearly point towards a PopIII-dominated GRB.

As expected, the different first star models have little effect on the distribution of the properties of PopII-dominated GRBII hosts (dotted red lines), since the PopII/I regime becomes dominant shortly after the onset of star formation. More specifically, most of the PopII-dominated GRBIIs are hosted in galaxies with $Z > 10^{-2.5}\,\mathrm{Z}_\odot$, with a peak at $Z = 10^{-1.5}\,\mathrm{Z}_\odot$. Their stellar mass spans the range $(10^5$–$10^{9.5})\,\mathrm{M}_\odot$, peaking around $10^{7.5}\,\mathrm{M}_\odot$. Finally, their SFR is in the range $(10^{-2.5}-10)\,\mathrm{M}_\odot\,\mathrm{yr}^{-1}$, with a peak at $10^{-0.5}\,\mathrm{M}_\odot\,\mathrm{yr}^{-1}$. These results are consistent with those found by Salvaterra et al. (2013) and seem to hold for all models.

The metallicity distribution of PopIII-dominated GRBII hosts (solid black lines) shares similar features among the three models. For example, all of them have a peak at $Z \sim 10^{-2}\,\mathrm{Z}_\odot$ and a second one in the range $Z \sim (10^{-4.6}-10^{-3.4})\,\mathrm{Z}_\odot$. The presence of the $Z \sim 10^{-2}\,\mathrm{Z}_\odot$ peak can be explained by residual PopIII star formation in the outskirts of already evolved galaxies (e.g. Tornatore et al. 2007b; Maio et al. 2010). These events can push metallicities close to PopII-dominated ones (red dotted lines). However, most PopIII-dominated GRBII hosts show metallicities lower than those of PopII-dominated hosts. In the VMSN and MSN models, the majority of other PopIII-dominated GRBIIs are in galaxies with very low metallicity ($Z \leq 10^{-4}\,\mathrm{Z}_\odot$), while in the RSN model the peak of the distribution is at $Z \sim 10^{-3.5}\,\mathrm{Z}_\odot$. This happens as the SFR of PopIII stars in the RSN model is much higher. Although the metal pollution is delayed, a large number of small mass PopIII stars can enrich the galaxies very fast and thus few galaxies have $Z < 10^{-4}\,\mathrm{Z}_\odot$. For all models, the probability to find a PopIII-dominated GRBII (dashed blue lines) becomes lower than 10 per cent in galaxies with $Z > 10^{-3}\,\mathrm{Z}_\odot$.

The stellar mass of PopIII-dominated GRBII hosts in all models is distributed mainly within the range $(10^{4.5}-10^{7.5})\,\mathrm{M}_\odot$, lower than that of PopII-dominated GRBII hosts. However, while in the

VMSN and MSN models a peak is present at $M_* \sim 10^{6.5}\,M_\odot$, in the RSN model ∼60 per cent of PopIII-dominated GRBIIs are found in galaxies in the lower stellar mass of the range, i.e. $(10^{4.5}-10^{6})\,M_\odot$, with a prominent peak at $10^5\,M_\odot$. For any stellar mass, the probability of a given galaxy to host PopIII-dominated GRBIIs is very low in the VMSN and MSN model, i.e. PopIII-dominated GRBIIs are not sensitive to the stellar mass of their hosts. In the RSN model, instead, galaxies with $M_* < 10^5\,M_\odot$ only host PopIII-dominated GRBIIs. In fact, metal enrichment from PopIII stars in the RSN model is weaker and delayed (stellar lifetimes are up to 10 times longer than for VMSN), resulting in the survival of more pristine stars.

The three models also have similar SFR distributions for PopIII-dominated GRBII hosts. The most populated range is $(10^{-3}-10^{-0.5})\,M_\odot\,yr^{-1}$, with a peak at $\sim 10^{-2}\,M_\odot\,yr^{-1}$, about 1 dex lower than that of PopII-dominated GRBII hosts. In all models, the probability of hosting PopIII-dominated GRBIIs goes from 80 per cent for galaxies with SFR $< 10^{-3}\,M_\odot\,yr^{-1}$ to 5 per cent for those with SFR $> 10^{-2}\,M_\odot\,yr^{-1}$, with only a few PopIII-dominated GRBIIs in galaxies with SFR $> 1\,M_\odot\,yr^{-1}$.

4 DISCUSSION AND CONCLUSIONS

In this work, we have studied the first star signatures on metal abundance ratios measured in high-z GRB afterglow observations using N-body hydrodynamical cosmological simulations. The numerical simulations include a detailed chemical evolution, gas cooling and metallicity-dependent star formation. We run three simulations, which differ only for the models for first stars (and thus the associated metal enrichment): (i) a VMSN model with mass range [100, 500] $M_\odot$ in which metal pollution is driven by PISN with [140, 260] $M_\odot$; (ii) an MSN model with mass range [0.1, 100] $M_\odot$ where metals are produced by SNe with [10, 100] $M_\odot$; and (iii) an RSN model which is the same as the MSN model, but here the enrichment is done by SNe with masses of [10, 40] $M_\odot$.

Our calculations are based on a few implicit assumptions that deserve some critical discussion as, in principle, they can affect the final results. In particular, from the point of view of the stellar properties, the PopIII SFR may be slightly changed by the particular critical metallicity adopted in the range $\sim(10^{-6}-10^{-3})\,Z_\odot$, without altering the overall cosmic SFR and the PopII/I SFR. In addition, different stellar structure models may shift the resulting abundance ratios, although no major changes are expected, especially at low metallicities (see discussion in e.g. Maio & Tescari 2015). In fact, a number of physical processes in stellar cores (differential rotation, the initial composition, magnetic fields, nuclear reaction rates, explosion mechanisms, etc.) may affect theoretical metal yields, although their specific values are not expected to change significantly cosmic gas evolution, the fraction of GRBIIs in a PopIII-dominated medium, and the properties of GRBII host galaxies. Indeed, and mostly at early times, metallicities are dominated by oxygen, for which fairly solid constraints exist. Differently, the abundance ratios of PopIII-dominated GRBIIs are sensitive to the predicted metal yields from PopIII stars. For example, massive first stars (i.e. with mass $> 40\,M_\odot$ in the MSN model) can explode both as faint SNe and hypernovae, depending on the angular momentum of the resulting BH (Nomoto et al. 2013). The former case produces small heavy element yields (e.g. iron; Heger & Woosley 2010; Nomoto et al. 2013), which could explain the abundance ratios of carbon-enriched metal-poor (CEMP) stars observed in our Milky Way. In this case, PopIII-dominated GRBIIs in our MSN model can be identified with the abundance ratios and used to study first stars. The latter case has higher silicon and iron yields, and could be the reason for carbon-unenhanced metal-poor stars (Umeda & Nomoto 2005). Their abundance ratios are very similar to those of PopII/I stars, thus it would be difficult to separate those PopIII-dominated GRBIIs from the PopII-dominated ones. Finally, a different PopIII IMF slope may have an effect on the abundance ratio distributions, especially in the MSN model, by shifting the peak distribution discussed in Section 3.2. However, the ranges of abundance ratios that we focus on are only mildly affected, as they are mainly driven by the adopted SN mass range (Maio et al. 2010). We should additionally note that physical processes in the ISM are described by means of subgrid models, which have also been tested through simulations of isolated objects (e.g. Maio et al. 2013b). The effects of changing specific model parameters have been shown to be mild for star formation and enrichment, as long as the gas cooling is properly accounted for both atomic and molecular phases, as in our simulations.

Most of our results are weighted by the GRBII rates in the gas particles of the corresponding classes. We have considered that most PopIII stars are located either in the outskirts of massive galaxies (Tornatore, Ferrara & Schneider 2007a) or in low-mass galaxies (Maio et al. 2011, 2016; Wise et al. 2012; Biffi & Maio 2013), i.e. further away from the typical location of PopII stars. This means that GRBIIs exploding in these environments are more likely to retain information from PopIII rather than from PopII/I stars. A weighting by other properties, e.g. the gas or the metal mass of the particles, would give results very similar to those we have presented, especially concerning the criteria to identify the first star signal.

Theoretically, the amplitude of metal absorption lines depends on the GRB afterglow luminosity, the spectral shape and also the ionization status of the ISM. To investigate this in more detail, one would need to model the luminosity and spectrum of the afterglow (e.g. Ciardi & Loeb 2000), as well as the ionization status and dust fraction of the interstellar gas at very high resolution (Mancini et al. 2015, 2016; Bocchio et al. 2016). This is beyond the scope of this paper.

Compared to recent afterglow observations of high-z GRBs, e.g. GRB 111008A (Sparre et al. 2014) and GRB 130606A (Hartoog et al. 2015), we find that most of the absorption lines of carbon, oxygen, silicon and iron (except several Fe lines) would be observable even at $z > 10$ with VLT/X-Shooter.

We highlight that we have defined the dominance of a population according to the fraction of heavy elements coming from PopIII stars, $f_{\rm III}$, with PopIII- and PopII-dominated regimes having $f_{\rm III} > 60$ per cent and $f_{\rm III} < 20$ per cent, respectively. Nevertheless, we have verified that the exact boundaries used for our classification (within ±10 per cent variations) do not have a relevant impact on the final outcome.

We can summarize our main results as follows.

(i) The fraction of second-generation GRBs exploded in a medium enriched by PopIII stars (PopIII-dominated GRBIIs) is independent from the adopted first stars model. This fraction rapidly decreases with redshift, accounting for ∼30 per cent of GRBII at $z = 15$, 10 per cent at $z = 10$, but only 1 per cent at $z = 6$. Since the PopII SFR is almost independent from the mass spectrum of PopIII stars, also the observable rate of PopIII-dominated GRBIIs is hardly affected by it.

(ii) We have explored the possibility to identify PopIII-dominated GRBIIs from observations of abundance ratios. Although not very efficient, a single ratio could in principle be enough to select

PopIII-dominated GRBIIs in the VMSN and MSN model. In the former case, a unique signature is represented by a high [Si/C] ratio, i.e. [Si/C] > 0.7. In the latter, PopIII-dominated GRBIIs can be identified by [Fe/O] < -1.6, [Si/O] < -1, or [Fe/C] < -0.8.

(iii) PopIII-dominated GRBIIs are more easily selected using two abundance ratios. For MSN or VMSN models, the probability distribution shows memory of the adopted IMF, allowing us to distinguish the two. In the VMSN model, PopIII-dominated GRBIIs are found at [Si/O] > 0.67 [C/O] $+ 0.57$ or [Fe/C] > -1.1 [Si/C] $+ 0.72$, whereas in the MSN model, at least 70 per cent of them are within the limits of [Si/O] < 0.83 [C/O] $- 0.38$ or [Fe/C] < -1.6 [Si/C] $- 0.54$. On the other hand, as metal yields from PopIII SN explosions in the RSN model are very similar to those of PopII/I SNe, in this case it is not feasible to distinguish PopIII- from PopII-dominated GRBIIs.

(iv) The properties of galaxies hosting PopIII-dominated GRBIIs are not strongly affected by the assumption on the mass of the first stars. Generally, these galaxies have metallicity ($10^{-4.5}-10^{-1}\,Z_{\odot}$), stellar mass ($10^{4.5}-10^{7.5}\,M_{\odot}$) and SFR ($10^{-3}-10^{-0.5}\,M_{\odot}\,yr^{-1}$), all lower than those of the normal PopII-dominated GRBII hosts (in agreement with Ma2015). Additionally, the GRBIIs observed in host galaxies with $Z < 10^{-4}\,Z_{\odot}$ are most likely PopIII-dominated.

(v) Finally, we would like to mention that none of the GRBs detected so far at $z = 5$–6 shows abundance ratios favouring a PopIII-dominated environment (see Ma2015 for a case by case discussion). This is consistent with the expected fraction of PopIII-dominated GRBIIs in this redshift range, i.e. $\sim 10^{-2}$.

ACKNOWLEDGEMENTS

We acknowledge the anonymous referee for careful reading and very helpful comments that improving the presentation of the results. QM is also partially supported by the National Natural Science Foundation of China (Grant no. 11373068 and no. 11322328), the National Basic Research Program ('973' Program) of China (Grants no. 2014CB845800 and no. 2013CB834900), and the Strategic Priority Research Program 'The Emergence of Cosmological Structures' (Grant no. XDB09000000) of the Chinese Academy of Sciences. We used the tools offered by the NASA Astrophysics Data Systems and by the JSTOR archive for bibliographic research.

REFERENCES

Asplund M., Grevesse N., Sauval A. J., Scott P., 2009, ARA&A, 47, 481
Becker G. D., Sargent W. L. W., Rauch M., Carswell R. F., 2012, ApJ, 744, 91
Biffi V., Maio U., 2013, MNRAS, 436, 1621
Bocchio M., Marassi S., Schneider R., Bianchi S., Limongi M., Chieffi A., 2016, Proc. conf. Supernova Remnants: An Odyssey in Space after Stellar Death. Chania, Greece, 134. Available at: http://snr2016.astro.noa.gr
Bromm V., Loeb A., 2002, ApJ, 575, 111
Caffau E. et al., 2011, Nature, 477, 67
Campisi M. A., Maio U., Salvaterra R., Ciardi B., 2011, MNRAS, 416, 2760
Castro-Tirado A. J. et al., 2013, A&A, preprint (arXiv:1312.5631)
Ciardi B., Loeb A., 2000, ApJ, 540, 687
Clark P. C., Glover S. C. O., Smith R. J., Greif T. H., Klessen R. S., Bromm V., 2011, Science, 331, 1040
Cucchiara A. et al., 2011, ApJ, 736, 7
de Souza R. S., Yoshida N., Ioka K., 2011, A&A, 533, A32
de Souza R. S., Ciardi B., Maio U., Ferrara A., 2013a, MNRAS, 428, 2109
de Souza R. S., Mesinger A., Ferrara A., Haiman Z., Perna R., Yoshida N., 2013b, MNRAS, 432, 3218
Elliott J., Khochfar S., Greiner J., Dalla Vecchia C., 2015, MNRAS, 446, 4239
Ghirlanda G. et al., 2015, MNRAS, 448, 2514
Hartoog O. E. et al., 2015, A&A, 580, A139
Heger A., Woosley S. E., 2002, ApJ, 567, 532
Heger A., Woosley S. E., 2010, ApJ, 724, 341
Inoue S., Salvaterra R., Choudhury T. R., Ferrara A., Ciardi B., Schneider R., 2010, MNRAS, 404, 1938
Kawai N. et al., 2006, Nature, 440, 184
Koopmans L. et al., 2015, Proc. Sci., The Cosmic Dawn and Epoch of Reionisation with SKA. SISSA, Trieste, PoS#001
Ma Q., Maio U., Ciardi B., Salvaterra R., 2015, MNRAS, 449, 3006 (Ma2015)
Maio U., 2011, Class. Quantum Grav., 28, 225015
Maio U., Barkov M. V., 2014, MNRAS, 439, 3520
Maio U., Tescari E., 2015, MNRAS, 453, 3798
Maio U., Viel M., 2015, MNRAS, 446, 2760
Maio U., Dolag K., Ciardi B., Tornatore L., 2007, MNRAS, 379, 963
Maio U., Ciardi B., Dolag K., Tornatore L., Khochfar S., 2010, MNRAS, 407, 1003
Maio U., Khochfar S., Johnson J. L., Ciardi B., 2011, MNRAS, 414, 1145
Maio U., Salvaterra R., Moscardini L., Ciardi B., 2012, MNRAS, 426, 2078
Maio U., Ciardi B., Müller V., 2013a, MNRAS, 435, 1443
Maio U., Dotti M., Petkova M., Perego A., Volonteri M., 2013b, ApJ, 767, 37
Maio U., Petkova M., De Lucia G., Borgani S., 2016, MNRAS, 460, 3733
Mancini M., Schneider R., Graziani L., Valiante R., Dayal P., Maio U., Ciardi B., Hunt L. K., 2015, MNRAS, 451, L70
Mancini M., Schneider R., Graziani L., Valiante R., Dayal P., Maio U., Ciardi B., 2016, MNRAS, 462, 3130
Nagamine K., Zhang B., Hernquist L., 2008, ApJ, 686, L57
Nomoto K., Kobayashi C., Tominaga N., 2013, ARA&A, 51, 457
Salvaterra R., 2015, J. High Energy Astrophys., 7, 35
Salvaterra R., Chincarini G., 2007, ApJ, 656, L49
Salvaterra R. et al., 2009, Nature, 461, 1258
Salvaterra R. et al., 2012, ApJ, 749, 68
Salvaterra R., Maio U., Ciardi B., Campisi M. A., 2013, MNRAS, 429, 2718
Schneider R., Ferrara A., Natarajan P., Omukai K., 2002, ApJ, 571, 30
Schneider R., Ferrara A., Salvaterra R., Omukai K., Bromm V., 2003, Nature, 422, 869
Simcoe R. A., Sullivan P. W., Cooksey K. L., Kao M. M., Matejek M. S., Burgasser A. J., 2012, Nature, 492, 79
Sparre M. et al., 2014, ApJ, 785, 150
Springel V., 2005, MNRAS, 364, 1105
Stacy A., Bromm V., 2014, ApJ, 785, 73
Suda T., Fujimoto M. Y., 2010, MNRAS, 405, 177
Suwa Y., Ioka K., 2011, ApJ, 726, 107
Takahashi K., Inoue S., Ichiki K., Nakamura T., 2011, MNRAS, 410, 2741
Tanvir N. R. et al., 2009, Nature, 461, 1254
Thielemann F.-K. et al., 2003, Nucl. Phys. A, 718, 139
Toma K., Sakamoto T., Mészáros P., 2011, ApJ, 731, 127
Tornatore L., Ferrara A., Schneider R., 2007a, MNRAS, 382, 945
Tornatore L., Borgani S., Dolag K., Matteucci F., 2007b, MNRAS, 382, 1050
Umeda H., Nomoto K., 2005, ApJ, 619, 427
van den Hoek L. B., Groenewegen M. A. T., 1997, A&AS, 123, 305
Wise J. H., Turk M. J., Norman M. L., Abel T., 2012, ApJ, 745, 50
Woosley S. E., Weaver T. A., 1995, ApJS, 101, 181

This paper has been typeset from a TEX/LATEX file prepared by the author.